Magnetic excitations around magnetic Brillouin zone centre in antiferromagnetic Mn(13.7%Ni) alloy

1997 J. Phys.: Condens. Matter 9 10761

(http://iopscience.iop.org/0953-8984/9/48/018)

J. Phys.: Condens. Matter **9** (1997) 10761–10776. Printed in the UK PII: S0953-8984(97)83005-6

Magnetic excitations around magnetic Brillouin zone centre in antiferromagnetic Mn(13.7%Ni) alloy

J Jankowska-Kisielinska, K Mikke and J J Milczarek
Institute of Atomic Energy, 05-400 Otwock, Świerk, Poland

Received 26 March 1997, in final form 24 July 1997

Abstract. Our studies of the itinerant antiferromagnetic γ-Mn-based alloys are extended to investigate magnetic excitations in a Mn(13.7%Ni) alloy. The composition of the present sample being close to the part of the phase diagram where a number of structural phase transitions take place, the basic aim of this work is the search for the effect of these transitions on spin dynamics. This is the first study of the Mn–Ni alloy in the fct ($c < a$) phase. The parameters of the spin wave dispersion relation and their temperature dependence are determined and compared with those for Mn–Ni alloys in the fct ($c > a$) and fcc phases. We obtain the concentration dependence of the low-temperature parameters of the spin wave dispersion relation which differs essentially from that found for the Mn–Fe alloys. In particular the change of the spin wave parameters in the vicinity of the phase transitions in Mn–Ni alloys is remarkable.

1. Introduction

For the past four decades one of the most challenging problems in condensed state physics has been the nature of magnetism in 3d metals and their alloys. They are the unique magnetic systems where the magnetic ordering is determined by the behaviour of the conduction electrons. In order to identify the interactions responsible for their specific features the studies of their magnetic microdynamics were started by inelastic neutron scattering (INS). The INS cross section being directly related to the generalized frequency and wavevector-dependent susceptibility $\chi(\boldsymbol{q}, \omega)$, which can be measured in principle over the whole $(\boldsymbol{q}, \omega)$-space, the full description of the microdynamics of a magnetic system is possible. In the case of ferromagnetic alloys these studies allowed us to obtain most of their characteristics and the theoretical treatment of these data was also fairly successful. In the case of antiferromagnetic 3d metals, chromium and manganese, both a satisfactory set of experimental data and their theoretical treatment are still lacking.

Band theory does not, as yet, allow us to answer the interesting question regarding the analogy of manganese to chromium. Magnetic excitations in chromium and its alloys were found to be very complex. The close nesting of the responsible electron energy bands in chromium gives rise to the very specific behaviour of the magnetic excitations. Spin waves (SWs) in chromium were found to have very high energies and, in fact, they are not yet clearly identified. The nature of SWs in manganese seems to be different.

The main features of the antiferromagnetism of manganese alloys are their SW velocities corresponding to high-exchange energies, strong SW damping, large SW energy gaps at long SW wavelengths and non-integral moments between 1 and $2.3\mu_B$. At high Mn concentrations the magnetic transition is accompanied by a structural fcc $\leftrightarrow$ tetragonal

0953-8984/97/4810761+16$19.50

martensitic transition anticipated by strong elastic constant softening (Lowde *et al* 1981, Sato *et al* 1981).

The γ-Mn cannot be studied in pure metal since it is not stable below 1470 K. A non-magnetic β-phase is stable above 727 K, and bcc α-phase below this temperature with a rather complicated antiferromagnetic structure below 98 K (see e.g. Bozorth 1951, Oleś *et al* 1976). Fortunately by alloying Mn with a number of elements, for example Fe, Ni, Cu, Ge, Ga the γ-phase can be stabilized, and the expectation is that the properties of pure γ-Mn can be obtained by extrapolation of the obtained concentration dependence of the desired characteristics. Extrapolation for several impurities is needed since the concentration dependence of the properties of different alloys is different. SWs in manganese alloys have been studied for nearly 20 years. The results for Mn–Fe and Mn-Cu were summarized by Holden *et al* (1992).

Our studies of tetragonal γ-Mn alloys also had a more extended motivation. The idea was the study of the magnetic phase transitions in γ-Mn alloys, and their suggested connection to (or even a driving force function of?) the structural phase transitions, which in turn are responsible for the shape memory effects occurring in some of these alloys.

The original aim of the present work was the investigation of SWs in the orthorhombic phase of the antiferromagnetic Mn–Ni alloy. This phase was identified in our sample by means of x-ray diffraction, but detailed neutron diffraction measurements have revealed that the contribution of this phase does not exceed 10% of the sample volume and the main part of the sample has the fct ($c < a$) structure. The unavoidable chemical inhomogeneity of the sample resulting from the single crystal growth process and the fact that the orthorhombic phase appears only in a narrow concentration range leaves little chance for growing a single crystal of a reasonable size. Since magnetic excitations in the fct ($c < a$) phase of the Mn–Ni alloys were not measured before the detailed investigation of this alloy was decided, the more so that the proximity of the structural phase transition makes such a study very interesting.

The studies of the itinerant antiferromagnetic γ-Mn-based alloys are now extended to the investigations of magnetic excitations in a Mn(13.7%Ni) alloy. This is the first study of the Mn–Ni alloy in the fct ($c < a$) phase. The parameters of the SW dispersion relation and their temperature dependence were determined and compared with those for other Mn–Ni alloys. These data are discussed in terms of the presently available theoretical models. The composition of the present sample being close to this part of the phase diagram where a number of structural phase transitions take place, the basic aim of this work is to look for the effect of the structural phase transitions on spin dynamics.

2. Crystal and magnetic structures of γ-Mn alloys

At high Mn concentrations the antiferromagnetic transition in many fcc alloys is accompanied by a deformation of their crystal lattice. A sequence of phase transitions appears as illustrated by the phase diagram displayed in figure 1 for the Mn–Ni system (Honda *et al* 1976). At the highest Mn concentration one of the axes is shortened (fcc–fct with $c < a$). Later, in a rather limited Mn concentration range, shortening of two axes takes place: different in two directions—the orthorhombic phase, or equal in two directions—the fct phase with $c > a$. At still lower Mn content the fcc structure remains unchanged after the transition to antiferromagnetic structure. A similar phase diagram was observed for the Mn–Fe system (Vintaykin *et al* 1985). The main difference is the shift of the phase boundaries between different sub-phases to the lower Mn concentration in Mn–Fe alloy.

This sequence of four crystallographic phases might be ascribed to a sequence of

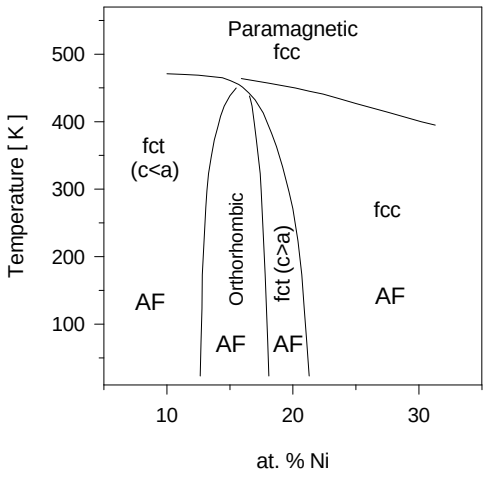

Figure 1. Phase diagram for the Mn–Ni system after Honda *et al* (1976).

multiple spin density waves (MSDW) (Long and Yeung 1986). In the general case the magnetic structure can be described by the sum of three longitudinal commensurate spin density waves (SDW) with the wavevectors oriented along three main crystal axes and with different amplitudes. If only one component is present we have the single SDW (SSDW) and it is connected with the fct phase with $c < a$. If there are two components with the same amplitude we have the double SDW (DSDW), which is connected to the fct phase with $c > a$. Three components with equal amplitudes create the triple SDW (TSDW)—connected to the cubic phase. These three cases are the simplest, they have one order parameter. There are also possible states with two order parameters. The orthorhombic SDW (OSDW) with two components with different amplitudes corresponds to the orthorhombic phase. The augmented SDW (ASDW)—with three components with two equal amplitudes and one different corresponds to the fct phase with a c/a ratio depending on the ratio of the amplitudes. Finally, the general SDW (GSDW) is considered, which has three components with three different amplitudes, i.e. it has three order parameters.

Since the lattice deformations are smaller than 5% the notation 'fct' for the tetragonal structure is used in the literature of the subject (e.g. Honda *et al* 1976) to emphasize its similarity to the fcc structure. The nuclear Bragg reflexes obtained from deformed lattices are only slightly shifted from their positions for the fcc lattice. Also all the above-mentioned magnetic structures studied by neutron scattering on polydomain samples give magnetic Bragg reflexes at similar superstructure positions shifted only in the case of the shortening of the lattice parameters. The pseudo-fcc notation for the reciprocal lattice is used in the literature.

It is only in the fct ($c < a$) structure that one can prove by neutron diffraction for single domain samples what is the type of the antiferromagnetic structure and that it is the SSDW structure. For other structures neutron diffraction does not allow us to distinguish between multi-SDW structures and a mixture of domains with SSDW (Ishikawa 1975). The TSDW structure was identified by γ-ray emission from spin-polarized nuclei in the fcc Mn–Ni alloy (Kawarazaki *et al* 1988). Other structures: DSDW, OSDW and ASDW were not verified directly until now.

Many theoretical descriptions were developed in order to find the cause of the phase transitions between these states. The earlier attempts (e.g. Cade and Young 1980) were based

on the rigid band model and the main role was played by the change of the electron/atom ratio with alloy concentration. Instabilites occur when Fermi surface nesting becomes nearly perfect.

Recently Oguchi and Freeman (1984) showed that a variation of the c/a ratio in γ-Mn for constant volume leads to a minimum of the total energy for $c/a = 0.90$ and an antiferromagnetic moment of about $2.3\mu_B$. These results, however, have been obtained for a volume of 12.94 Å^3, which is 3.5% larger than the experimental value. The new band theoretical study (Duschanek *et al* 1989) employs the augmented spherical wave method. Effects of exchange and correlation are treated within the local spin-density approximation. The tetragonal distortion was shown to stem from the onset of magnetism and total energy was obtained as a function of the c/a ratio. Paramagnetic phase was shown to have its minimum for the fcc phase and the antiferromagnetic phase for $c/a = 0.94$.

One of the attempts of an explanation of the phase diagram is the work of Jo and Hirai (1986). The fact that the temperature of the structural phase transition is always equal to or less than T_N seems to suggest the importance of a magnetoelastic coupling. On the basis of the Landau expansion, they have shown that the coupling between suitable magnetic order parameters and strains leads to the above-mentioned phase diagrams. The simple magnetoelastic interaction allows us to link the presence of the MSDW states to different lattice structures in such a way that the phase diagrams of the manganese alloys could be explained. The line of the first-order phase transitions from the paramagnetic fcc to antiferromagnetic fct states and the tricritical point on the phase diagrams of Mn-rich alloy were obtained.

Long and Yeung, in series of works summarized by Yeung (1988), examined the transitions between the various MSDW states. The total energy calculations within the Hartree–Fock approximation for SSDW, DSDW and TSDW for various electron/atom ratios and bandwidths allowed them to explain the first-order phase changes. The susceptibility calculations allowed a complementary description of the continuous phase transitions. The spin orientation phase transitions were predicted and the phonon softening near this transition was explained.

Recently, Long and Bayri (1993) emphasized the alloy disorder as the decisive factor. They studied the problem in classical Heisenberg model by perturbation method. The model predicts the amounts of energy available for different MSDW states from isolated impurity. The effect depends first on the sort of impurity (magnetic or non-magnetic) and secondly on the presence or absence of the local field at sites of substitution or of interstitial doping. Substitution of non-magnetic impurities into γ-Mn is expected to destabilize the collinear ground state. The reason is that the polarization cloud surrounding the impurity spreads out further and more effectively in a non-collinear state. In this way, treating Ni as a non-magnetic impurity, the phase diagram of γ-Mn–Ni alloys can be explained.

3. Sample characteristics

The investigated sample, a single crystal in the form of a parallelepided, measuring: $19.6 \times 11.4 \times 9.6$ mm^3 was grown in the Institute of Metal Physics, Moscow, Russia. It is antiferromagnetic below $T_N = 480$ K. Its mosaic spread was $\eta = 110^\circ$. The sample composition, as obtained by chemical analysis, is 86.3 at% Mn and 13.7 at% Ni. The sample was investigated by x-ray difractometry and the orthorhombic phase was detected at room temperature. Since this result could not be clearly confirmed by neutron scattering, the detailed study was performed on the temperature dependence of the crystal lattice constants by x-ray diffraction. These measurements were performed in collaboration with Vintaikin in

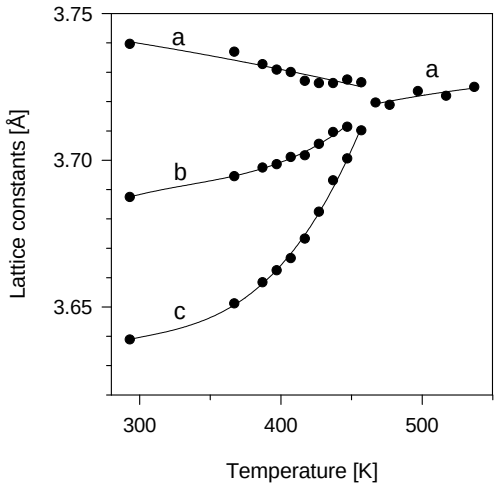

Figure 2. Temperature dependence of the lattice constants determined from x-ray diffraction measurements.

the Institute of Metal Physics, Moscow. The obtained temperature dependence of the lattice constants derived from Bragg angle values of (200), (020) and (002) reflections is shown in figure 2. These data demonstrate that $a \neq b \neq c$ between the room temperature and 460 K, but they could not be fully conclusive considering that x-ray diffraction results refer only to the sample surface, and only to a few small spots on the sample surface. In addition, the earlier x-ray studies of the structure of the Mn–Ni alloy performed on polycrystal samples (Vintaykin *et al* 1985, Honda *et al* 1976) indicated that the composition range in which the orthorhombic phase is realized is comparable with the composition spread measured in our sample. Based on these results no reliable estimate was possible of the volume fraction of the orthorhombic phase. The results of elastic neutron scattering refer nearly to the full volume of the sample. The measurements performed in the vicinity of (200), (020) and (002) rlp did not confirm the presence of three separated peaks. The full analysis of the neutron data indicated that only less than 10% of the sample volume is in the orthorombic phase, while its main part is in the fct ($c < a$) phase.

It should be emphasized that the crystal growth process of these alloys leads unavoidably to considerable inhomogeneity of the composition. The deviations from the nominal composition may reach even ± 3 at% Mn. By the electron microprobe study of our sample it was shown that the Mn concentration spread over regions measuring $\sim 2\ \mu\text{m}^2$ was ± 2.5 at% Mn.

An important feature of our sample is that it is polydomain. The population of the different types of domains with different c and a axes orientation must be known for proper planning of the experiment and for the data analysis. The population of different types of domains was obtained by measuring the intensities of all $\langle 110 \rangle$ type magnetic reflections and the corresponding nuclear reflections $\langle 220 \rangle$. The derived volume fractions of domains with wavevector of SDW (Q_{SDW}) along three main cubic directions are: 0.37 ± 0.05, 0.08 ± 0.02 and 0.55 ± 0.11.

The Néel temperature was established by measuring the temperature dependence of intensity of magnetic Bragg reflection (011) and of critical scattering at (001) and (010) rlp. The temperature dependence of the magnetic order parameter (the sublattice magnetization)

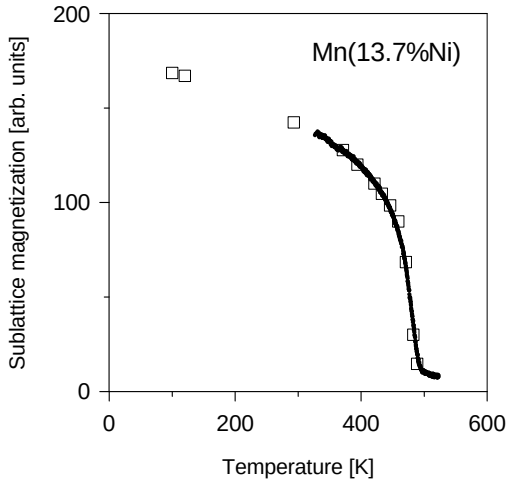

Figure 3. Temperature dependence of magnetic order parameter (sublattice magnetization $\propto \sqrt{I_{110}}$). Open squares represent the results of static measurements, small dots come from the measurements taken at the constant rate of the temperature changes.

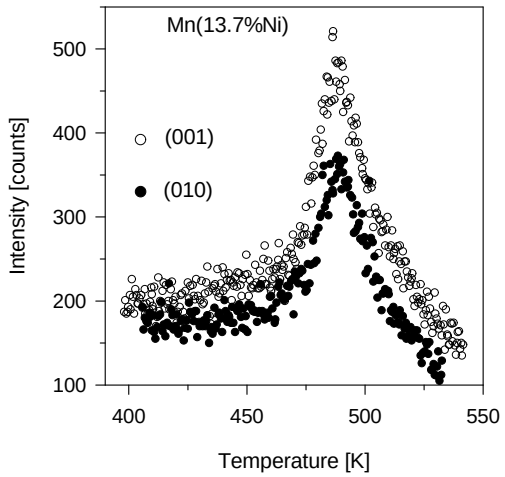

Figure 4. Temperature dependence of the elastic neutron scatterring intensity measured at the (001) and (010) rlp.

measured as the square root of the intensity of the (110) reflection is shown in figure 3. The temperature dependence of the intensity of neutrons scattered at (001) and (010) rlp is the same as shown in figure 4. The small difference in the scale is not significant, being probably due to different volume fractions of the sample exposed in these two cases. Below T_N the fraction of domains having Q_{SDW} parallel to the scattering vector is 37% at the (001) rlp and 8% at the (010) rlp. The SWs can be observed close to the (001) rlp but not close to the (010) rlp.

4. Experimental procedures

The measurements of neutron scattering by SWs were carried out by means of a triple axis spectrometer at the 10 MW EWA reactor at IEA Świerk. The horizontal collimation angles, starting from the reactor core were: 90′–10′–20′–200′ for most of the measurements. The vertical collimation angles were: 65′–142′–194′–364′. The preliminary measurements at 100 K indicated that the available scattered neutron intensities are too low to assure reasonable results with these collimations and the horizontal collimations had to be relaxed to 45′ and 50′ before and after the sample, correspondingly.

Since our sample was not a single-domain single crystal some precautions were necessary to take into account the contribution of different sets of domains. The inelastic neutron scattering was measured close to the (001) rlp with such a orientation of the sample that for 37% of the magnetic domains the SDW wavevector is parallel to the scattering wavevector. For these domains the (001) rlp lies in the centre of the Brillouin zone. The remaining 63% of the domains have their SDW wavevector perpendicular to the scattering wavevector.

While the desired domains (where the measurements had to be performed) were those with the centre of the magnetic Brillouin zone at the (001) rlp, there was also a contribution to the scattering originating from domains for which in this set-up the Brillouin zone boundary is approached. This additional contribution is significant for small energy transfers and rises with the increasing temperature. Our measurements were therefore supplemented by scans performed at the (010) rlp where the contribution of the domains having the centre of the magnetic Brillouin zone is negligible. In order to eliminate this second component for the $I(E)$ distributions at higher temperatures the background has been corrected by adding the intensity above the background measured at the (010) rlp corrected by the relative population of domains.

At 100 K the $I(E)$ distribution was measured at the incident neutron energy $E_0 = 25.6$ meV and $E_0 = 50$ meV. The energy resolution is much better for lower E_0, but the intensity is much lower. The calculated projection of the resolution elipsoid on energy axis for $E_0 = 50$ meV and energy transfer 8.25 meV is 4.42 meV and for $E_0 = 25.6$ meV and the same energy transfer is 1.26 meV. The obtained distribution for $E_0 = 50$ meV is shown in figure 5(a). The full curve is the result of the computed convolution of the neutron scattering cross section with the resolution function. The broken curve indicates the background. The momentum transfer distributions, $I(q)$, were measured at incident neutron

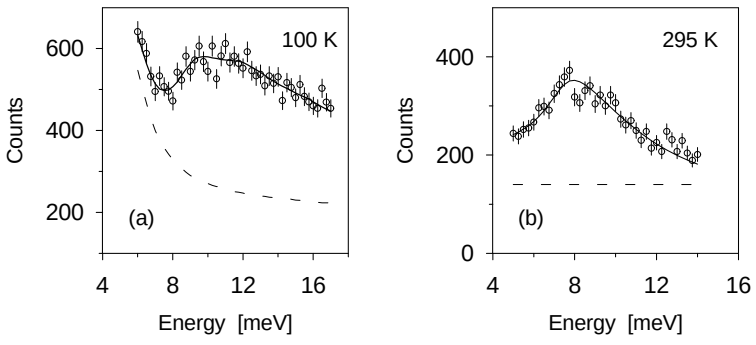

Figure 5. The intensity distributions versus energy transfer measured at (001) at (a) 100 K for $E_0 = 50$ meV and (b) 295 K for $E_0 = 25.6$ meV.

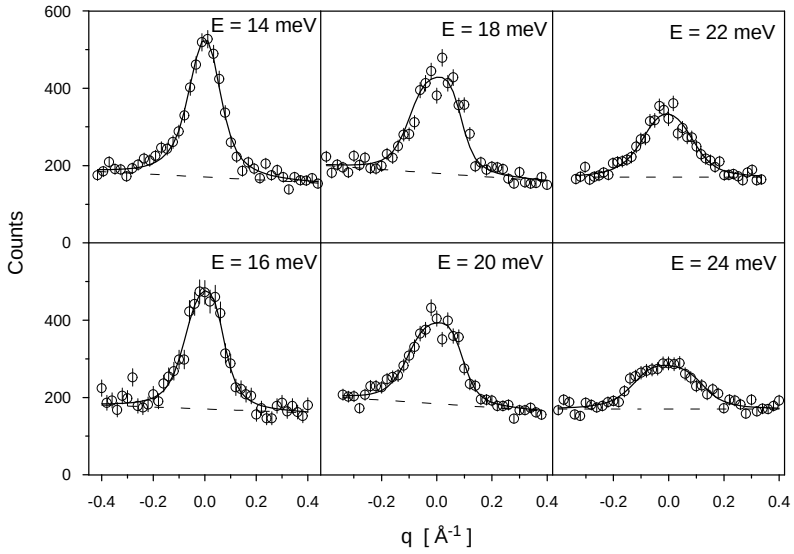

Figure 6. The intensity distributions versus momentum transfer measured at 100 K and for energy transfers 14, 16, 18 and 20 meV for $\boldsymbol{q} \parallel [001]$ and for energy transfers 22 and 24 meV for $\boldsymbol{q} \perp [001]$.

energy $E_0 = 50$ meV for constant energy transfers 14, 16, 18 and 20 meV with q parallel to the reciprocal lattice vector, and for 20, 22 and 24 meV with q perpendicular to it. For measurements around (001) with $E_0 = 50$ meV and energy transfer 20 meV the calculated projections of the resolution elipsoid on the directions parallel and perpendicular to [001] are 0.12 Å^{-1} and 0.16 Å^{-1} correspondingly. A set of the obtained $I(q)$ distributions is shown in figure 6. The full curves are the results of the computed convolution of the resolution function of the neutron spectrometer with the neutron scattering cross section for damped SWs. Additional measurements with a tight collimation were made with the zinc crystal analyser replaced by the pyrolitic graphite. These were the $I(E)$ and $I(q)$ scans for $E = 14$, 16, 20 and 22 meV with q parallel to the scattering wavevector. A considerable increase in the scattered intensities was obtained but it was unfortunately accompanied by much poorer resolution. The calculated projection of the resolution elipsoid on energy axis for $E_0 = 25.6$ meV and the energy transfer $E = 10$ meV is 1.72 meV. For measurements with $E_0 = 50$ meV and energy transfer 20 meV the calculated projection of the resolution elipsoid on the direction parallel to [001] is 0.16 Å^{-1}.

At room temperature and with $E_0 = 25.6$ meV the $I(E)$ and $I(q)$ distributions were obtained for 10 and 12 meV and at $E_0 = 50$ meV $- I(E)$ and $I(q)$ scans for $E = 14$, 18 and 20 meV with q parallel to the reciprocal lattice vector and for $E = 20$ and 22 meV with q perpendicular to it. The $I(E)$ distribution for $E_0 = 25.6$ meV is presented in figure 5(b) and the $I(q)$ distributions in figure 7. The full curves are the results of computation. The broken curves represent the background.

At higher temperatures the $I(E)$ scans were made with $E_0 = 25.6$ meV at 370, 420, 433, 446 and 459 K. The measured $I(E)$ distributions are presented in figure 8. For $E_0 = 50$ meV the $I(q)$ scans were made at 394, 420, 459, 471 and 483 K. Some measurements with a tight collimation but with the pyrolitic graphite analyser were also performed at higher temperatures. At 396 K the $I(q)$ distribution for $E = 10$ meV, at 433 K the $I(q)$ for $E = 12$, 14 and 16 meV, at 445 K the $I(q)$ for $E = 10$, 12, 14 and 16 meV and

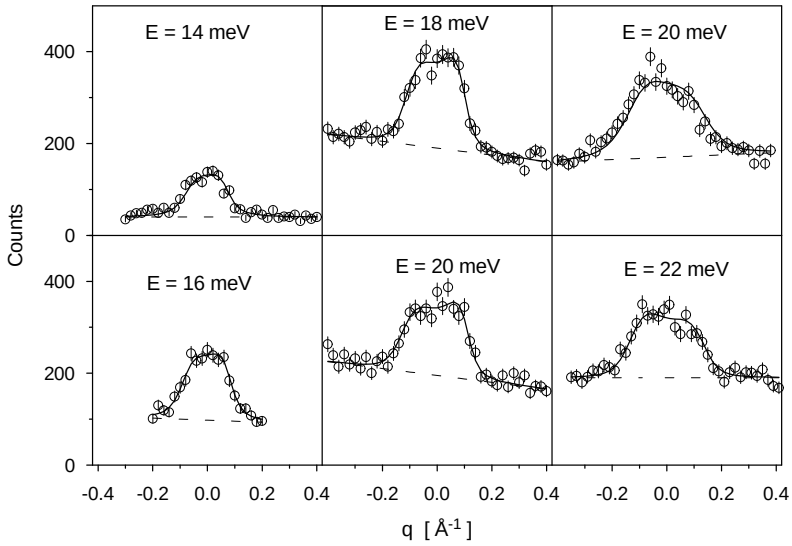

Figure 7. The intensity distributions versus momentum transfer measured at 295 K for $\boldsymbol{q} \parallel [001]$ with energy transfers 14, 16, 18 and 20 meV and for $\boldsymbol{q} \perp [001]$ with energy transfers 20 and 22 meV. The counting time for 14 meV was four and for 16 meV was two times shorter than for other energies.

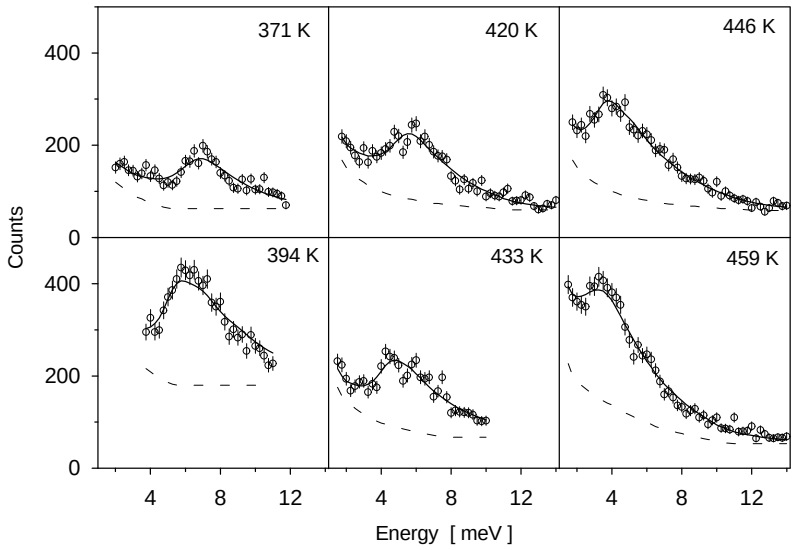

Figure 8. The intensity distributions versus energy transfer measured at (001) at different temperatures. The counting time at 394 K was twice as long as at other temperatures.

at 458 and 470 K the $I(q)$ for 12 meV. The $I(q)$ distributions for $E = 14$ meV for different temperatures are presented in figure 9. One can observe that the two distributions at highest temperatures (below and above the T_N) are very similar: they have nearly the same maximum intensity and the latter distribution is somewhat broader.

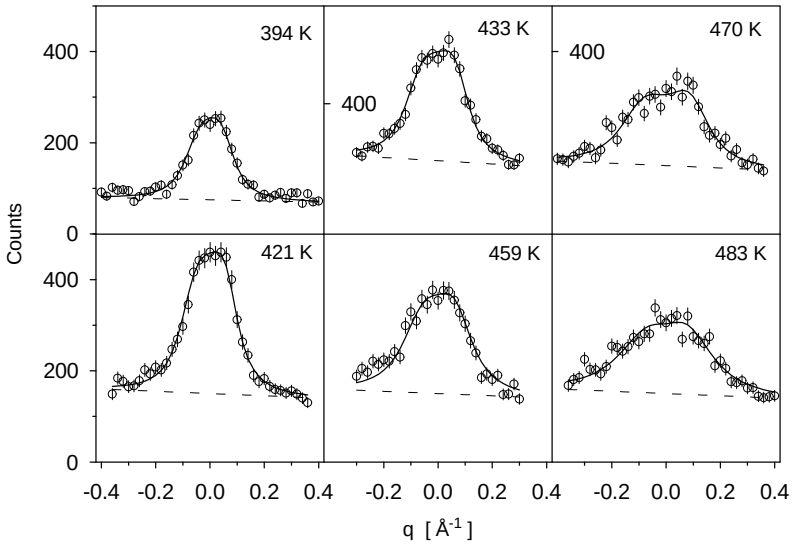

Figure 9. The intensity distributions versus momentum transfer measured for the energy transfer $E = 14$ meV at different temperatures. The counting time for the distributions for 394 and 433 K was half of that for other distributions. The distribution for 433 K was obtained with pyrolytic graphite analyser, while Zn analyser was used in other cases.

5. Theoretical description

The first theoretical description of SWs in an itinerant antiferromagnet at finite temperatures was given by Liu (1970) and it was for a simple model of Cr with the commensurate SDW. The next one, also for Cr, but both for the commensurate and incommensurate SDW was proposed by Sato and Maki (1974). Their result is somewhat different. Sato and Maki claimed that due to an error in Liu's calculations, his result does not obey the Goldstone theorem.

For temperatures smaller than $0.8T_N$ the resulting formula for the imaginary part of transverse susceptibility is similar in both papers and reads

$$\operatorname{Im}\chi_\perp(\boldsymbol{q},\omega) \propto \frac{\Gamma\omega}{(\omega^2 - E_q^2)^2 + \Gamma^2\omega^2} \tag{1}$$

where $E_q = vq$ is the SW energy and Γ is the damping parameter. In Liu's calculations Γ remains finite for $q \to 0$, Sato and Maki obtained Γ proportional to q^2. Liu obtained very strong damping at higher temperatures. Close to T_N the computed shape of $\operatorname{Im}\chi_\perp(\boldsymbol{q},\omega)$ cannot be described by any simple formula. In Sato and Maki's results damping is small for $q \to 0$ even in the vicinity of T_N and SW velocity can be derived in this region. It decreases with temperature proportionally to $(T - T_N)^{1/2}$.

In both cases the result above T_N corresponds to the critical fluctuations:

$$\operatorname{Im}\chi_\perp(\boldsymbol{q},\omega) \propto \frac{\omega}{(q^2 + \kappa^2)^2 + \alpha^2\omega^2} \tag{2}$$

where κ is the inverse correlation length and α is the inverse 'magnetic stiffness'.

Sato and Maki (1976) theoretically examined the spin excitations in the vicinity of T_N for γ-Mn–Fe with a TSDW. Below T_N the obtained formula for $\operatorname{Im}\chi_\perp(\boldsymbol{q},\omega)$ is similar to that for commensurate Cr, but the SW dispersion relation has another form: $E_q = \sqrt{v^2q^2 + E_g^2}$,

where E_g is the energy gap. The obtained SW velocity is proportional to the long-range order parameter M and E_g is proportional to M^2, both approaching 0 as $T \to T_N$. However, this treatment is not completely correct for an energy gap, since they introduced the dipole–dipole interaction. This interaction yields the energy gap in the SW dispersion which is observed experimentally in γ-Mn alloys, but it also causes the perpendicular polarization of SDW (magnetic moment perpendicular to Q_{SDW}) and this feature contradicts the experimental data for γ-Mn alloys. Thus the obtained temperature dependence of E_g has no meaning.

The calculations of the low-energy SW spectrum and damping for γ-Mn within the band model were first performed by Gillan (1973). A single SDW structure (SSDW) was assumed for the magnetic structure of manganese and the calculations were based on a realistic band structure, which reproduced very closely the magnetic moment $\mu = 2.332\mu_{\mathrm{B}}$. The poles of the generalized susceptibility were examined within RPA for small q, ω and for $T = 0$. No dependence on orbitals, i.e. the spherical shape was assumed for the exchange interaction. Spin–orbit coupling is usually suspected to be responsible for the energy gap in the SW spectrum. Its inclusion is, however, very laborious since 2×2 matrices should be replaced by those with 50×50 dimension and the expected error in the determination of the value of the energy gap would be much larger than the gap itself. The SW velocity for [001] and [100] directions were found to be 310 and 390 meV Å^{-1}. The damping was linearly dependent on q and the calculated proportionality factor was 50 meV Å^{-1}.

Basing on similar assumptions but allowing the dependence of the exchange interaction on orbitals Cade and Young (1977) obtained not only the poles of $\chi(\boldsymbol{q}, \omega)$ at $q \to 0$ but also a full dependence of χ on q for the [001] direction up to the BZ boundary. Two cases, one with a single exchange integral and another with five different integrals were investigated. The computed $\mu = 2.3\mu_{\mathrm{B}}$ is again very close to the experimental value and the features of the SW spectrum are quantitatively similar to those of Gillan and this is their good confirmation. Only for the five-orbital case is the obtained SW spectrum more complicated.

Since band calculation accuracy is not yet sufficient to calculate the SW energy gap, an attempt was made to understand it in the localized model (Holden *et al* 1992). The Hamiltonian used includes exchange interactions, quadrupolar interactions and magnetoelastic coupling between strains and quadrupoles. The obtained expression for the energy gap is as follows

$$E_g^2 = \left[\frac{36}{\sqrt{3}}\left(S+\frac{1}{2}\right)(K_{ME}+K_{QQ})\langle S_1^{\Gamma 3}\rangle\right] \times \left[-4SJ(120)+\frac{36}{\sqrt{3}}\left(S+\frac{1}{2}\right)(K_{ME}+K_{QQ})\langle S_1^{\Gamma 3}\rangle\right] \tag{3}$$

where $J(120)$ is the sum of the intersublattice exchange interactions, $K_{ME} = (B^{\Gamma 3})^2/24(C_{11}-C_{12})$, $B^{\Gamma 3}$ is the appropriate magnetoelastic coupling, C_{11} and C_{12} are the elastic constants, K_{QQ} is the mean of the quadrupolar interactions and $\langle S_1^{\Gamma 3}\rangle$ is the thermal expectation value of the quadrupole moment.

6. Data analysis and discussion

For data analysis the following formula based on formula (1) was used to describe the cross section for neutron scattering on SWs in an antiferromagnet:

$$\frac{\mathrm{d}^2\sigma}{\mathrm{d}\Omega\,\mathrm{d}E} \propto F^2(Q)[n(E)+1]\frac{\Gamma E}{(E^2-E_q^2)^2+\Gamma^2E^2} \tag{4}$$

where $n(E)$ is the population factor and $F(Q)$ is the magnetic form factor. SW energy follows the formula:

$$E_q^2 = v^2 q^2 + E_g^2 \tag{5}$$

where v is the SW velocity and $E_g = E(q = 0)$ is the energy gap in the SW spectrum. SW damping parameter Γ in these alloys has a linear dependence on the momentum transfer q

$$\Gamma = \Gamma_0 + \Gamma_1 \cdot q. \tag{6}$$

The parameters of the SW dispersion relation v and E_g and the damping parameters were derived by deconvolution procedures. The measured distributions $I(E)$ and $I(q)$ were computer fitted to the neutron spectrometer resolution function folded with the neutron scattering cross section. E_g is determined from the $I(E)$ distributions and v from the $I(q)$ scans. The value of Γ_0 was assumed constant (1 meV), and Γ_1 was determined from both $I(E)$ and $I(q)$ distributions.

The fitting of the $I(E)$ distribution obtained at 100 K for $E_0 = 50$ meV gave $E_g = 8.35 \pm 0.2$ meV and $\Gamma_1 = 56 \pm 11$ meV Å^{-1} with the assumption that $v = 230$ meV Å^{-1}. The weighted average values of the results for both $I(E)$ and $I(q)$ distributions obtained at 100 K with the collimations 45° and 50° are $v = 231 \pm 16$ meV Å^{-1} and $\Gamma_1 = 113 \pm 58$ meV Å^{-1}.

The fitting of the the $I(E)$ distribution measured at 295 K and at $E_0 = 50$ meV allowed us to derive $E_g = 7.4 \pm 0.2$ meV and $\Gamma_1 = 98 \pm 15$ meV Å^{-1} with the assumption that $v = 185$ meV Å^{-1}. The v and Γ_1 parameters were derived by the fitting procedure for the $I(q)$ distributions with $E_0 = 50$ meV for all measured E transfers and q directions at 295 K. The weighted average values of the parameters obtained from the above set of data are: $v = 192 \pm 7$ meV Å^{-1} and $\Gamma_1 = 72 \pm 19$ meV Å^{-1}. The same procedure was used to obtain the values of the parameters for higher temperatures.

For two highest temperatures we observe that $\Gamma_1 \leqslant v$ and this means the overdamping of SWs. Probably the formula used for the neutron scattering cross section does not apply to this temperature range. This result is consistent with that obtained by Wiltshire *et al* (1985) for the magnetic excitations in Mn–Cu above and below T_N. Above T_N and slightly below T_N they obtained a better fit for higher excitation energies with the damped SW formula (1), whereas for lower energies with fluctuations formula (2).

The temperature dependence of the SW velocity reduced to its value obtained at $T = 100$ K is shown in figure 10. The present data are compared with earlier data for Mn(17%Ni) (Jankowska-Kisielińska *et al* 1995) and for Mn(10%Fe,3%Cu) (Mikke *et al* 1992). The temperature dependence is very similar for these three alloys. The SW velocity reduced to its value obtained at $T = 100$ K, versus sublattice magnetization M is shown in figure 11. The sublattice magnetization is given in arbitrary units, and was derived as the square root of the integrated intensity at the (110) rlp measured at different temperatures. The full curve is a linear fit to the data. The linear dependence $v \propto M$ was predicted by Sato and Maki (1976). Our results, similarly to previous studies of the temperature dependence of SWs (Wiltshire *et al* 1985, Mikke *et al* 1992), at temperatures close to T_N do not confirm this prediction. In a lower temperature range the linear dependence is observed.

The temperature dependence of the energy gap of the SW spectrum at $q = 0$ reduced to the value obtained at $T = 100$ K is shown in figure 12. The present data are compared with the data for Mn(17%Ni) (Jankowska-Kisielińska *et al* 1995) and for Mn(10%Fe,3%Cu) (Mikke *et al* 1992). The energy gap for Mn(13.7%Ni) as a function of the sublattice magnetization at different temperatures is presented in figure 13. For the present alloy this dependence of E_g on magnetic order parameter differs somewhat from that obtained for different Mn–Fe alloys in the fcc phase (Tajima *et al* 1976) and for the Mn(10%Fe,3%Cu)

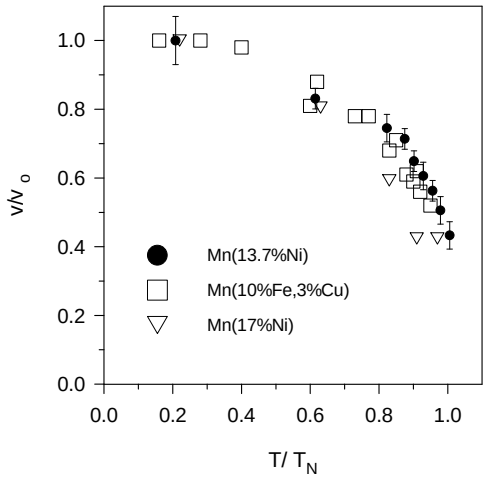

Figure 10. Temperature dependence of the SW velocity reduced to its value obtained at $T = 100$ K. The present data are compared with earlier data for Mn(17%Ni) (Jankowska-Kisielińska *et al* 1995) and for Mn(10%Fe,%Cu) (Mikke *et al* 1992).

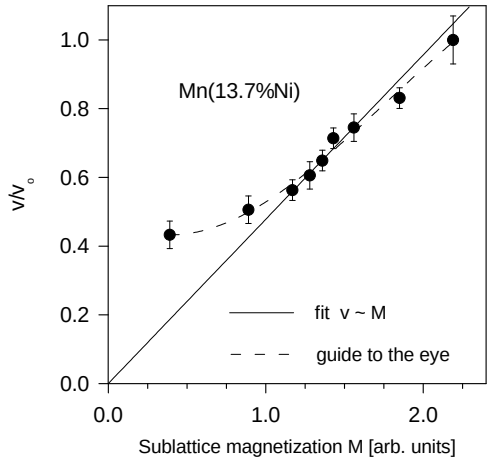

Figure 11. The SW velocity reduced to its value obtained at $T = 100$ K, versus the sublattice magnetization M. The full line is the linear fit. The broken curve is the guide to the eye.

alloy in the tetragonal ($c < a$) phase (Mikke *et al* 1992). In the Mn–Fe alloys the proportionality $E_g \propto M^x$ was obtained with $x = 1.5$ in both phases. In Mn(13.7%Ni) we obtained $x = 1.8 \pm 0.16$.

Our present low-temperature results may be compared with those obtained earlier for other Mn–Ni alloys. In the Mn(17%Ni) alloy with the fct ($c > a$) structure (Jankowska-Kisielińska *et al* 1995) the measurements were performed at 100, 295 K and at higher temperatures. In Mn–Ni alloys with the fcc structure the data are available for Mn(27%Ni) (Hennion *et al* 1976) at 295 K, for Mn(18%Ni) (Mikke *et al* 1987) at 295 K and for Mn(38%Ni) (Mikke *et al* 1989) at 100 K. These resuts are summarized in table 1.

The SW velocity decreases with Ni concentration and this decrease is much faster in the region of low Ni concentration compared with higher Ni content, where only the fcc phase exists. The dependence of the value of the SW energy gap on Ni concentrations for the above regions is much more pronounced than of the SW velocity. In the range of low Ni concentrations the energy gap has a fast decrease with increasing Ni concentration. Between 13.7%Ni (tetragonal $c < a$) and 17%Ni (tetragonal $c > a$) it goes down from 8.9 to 6 meV (for 100 K). In the range of higher Ni content, in the fcc phase, the dependence of E_g on concentration is weak.

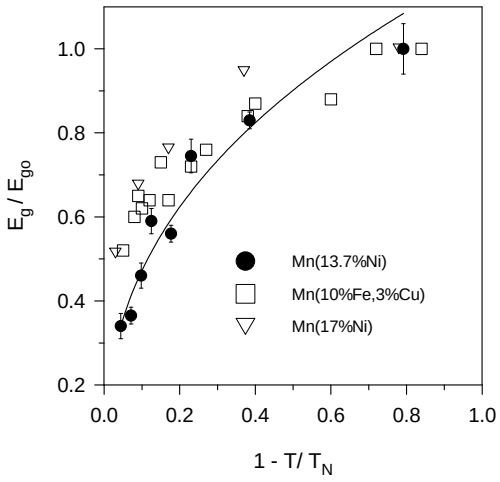

Figure 12. The temperature dependence of the energy gap of the SW spectrum at $q = 0$ reduced to the value obtained at $T = 100$ K. The present data are compared with the data for Mn(17%Ni) (Jankowska-Kisielińska *et al* 1995) and for Mn(10%Fe,3%Cu) (Mikke *et al* 1992). The full curve is the fit to the present data: $E_g/E_{g0} \propto (1 - T/T_N)^x$, $x = 0.4$.

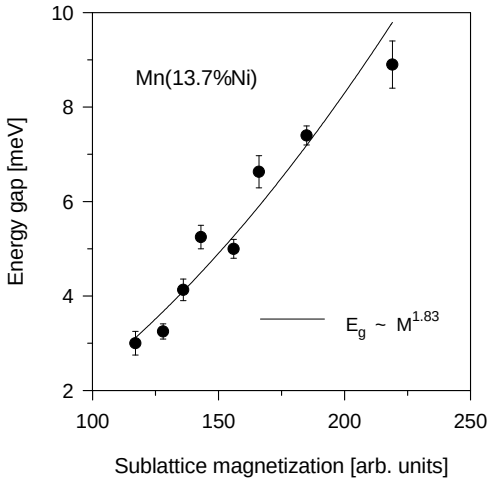

Figure 13. Energy gap for Mn(13.7%Ni) as a function of the sublattice magnetization at different temperatures.

Table 1. The parameters of the SW dispersion relation and damping at 100 and 295 K for different Ni concentrations in Mn–Ni alloys.

	v (meV Å^{-1})		E_g (meV)		Γ_1 (meV Å^{-1})	
%Ni	100 K	295 K	100 K	295 K	100 K	295 K
13.7	231 ± 16	192 ± 7	8.9 ± 0.5	7.4 ± 0.2	113 ± 58	72 ± 19
17	185 ± 12	175 ± 12	5.9 ± 0.2	4.8 ± 0.2	85 ± 15	110 ± 30
18	—	164 ± 12	—	4.8 ± 0.2	—	93 ± 30
27	—	201 ± 3	—	3.0 ± 0.3	—	$\sim 30\%$
38	140 ± 20	—	3.5 ± 0.5	—	—	—

This concentration dependence of the parameters of the SW dispersion relation differs essentially from that for the γ-Mn–Fe alloys, where these parameters are rather insensitive to both the Fe concentration and crystal phase changes (Mikke *et al* 1991, Tajima *et al* 1976). This difference is probably due to the fact that Ni introduces more perturbation than

Fe into the Mn matrix. Fe is the nearest neighbour of Mn in the periodic table with 3d electrons/atom, i.e. by one electron/atom more than Mn. The Fe impurity is magnetic in the Mn–Fe alloy. Pure fcc Fe is antiferromagnetic. The rigid band model predictions are fully justified in this case. Weak concentration dependence of the SW parameters is also consistent with the rigid band model.

On the other hand, Ni has eight 3d electrons/atom (by three more than Mn). Pure fcc Ni is ferromagnetic. Ni impurity is believed to carry no magnetic moment in Mn–Ni alloys and the magnetic moment perturbation extends to the nearest neighbours only for Mn(15%Ni) and to the third nearest neighbours in Mn(27%Ni) (Moze and Hicks 1979, 1982). For these reasons Long and Bayri (1993) studied theoretically the effect of the impurities and of the perturbations introduced by them on stability of different SDW phases of γ-Mn. They predicted that the paramagnetic impurity favours the non-collinear phases (DSDW, TSDW). The reason is that the polarization cloud around the impurity is more extended in non-collinear antiferromagnetic phases than in the collinear SSDW phase. We can also expect that perturbation introduced by paramagnetic Ni impurity, more extended in DSDW (fct with $c > a$) and TSDW (fcc), might be the reason for the remarkable change of the SW parameters in the region of the phase transitions in Mn–Ni.

7. Conclusions

We obtained the low-temperature values of the SW dispersion relation parameters for the Mn(13.7%Ni) alloy in the fct ($c < a$) phase. The SW velocity obtained at 100 K is 231 ± 16 meV Å^{-1}. This value is lower, but the same order of magnitude as predicted by the electron band calculations (Gillan 1973, Cade and Young 1977). The energy gap in the SW spectrum $E(q = 0)$ is 8.35 ± 0.2 meV at 100 K. The SW damping parameter, being the coefficient of q dependence of the reciprocal lifetime is $\Gamma_1 = 113 \pm 58$ meV Å^{-1} for 100 K.

The obtained values complete our studies of the concentration dependence of the SW parameters in Mn–Ni alloy in the region of the phase boundaries between different subphases of the γ-phase. The phase diagram of γ-Mn–Ni alloy is very similar to that for Mn–Fe but the concentration dependence of the parameters of the SW dispersion relation for the γ-Mn–Ni alloys differs essentially from that for the γ-Mn–Fe alloys (Mikke *et al* 1991, Tajima *et al* 1976). In Mn–Ni the change of the SW parameters in the vicinity of the phase transitions region is remarkable.

This difference is probably due to the difference between magnetic Fe impurity and non-magnetic Ni impurity, inducing magnetic perturbation of surrounding Mn atoms. This conclusion is consistent with the data on magnetic defects in Mn–Ni alloys (Moze and Hicks 1979, 1982) and the idea of Long and Bayri (1993) that the magnetic defect does induce the phase transition in Mn–Ni alloys.

The temperature dependence of SW parameters obtained in the Mn(13.7%Ni) is similar to the earlier results for Mn–Fe alloys (Tajima *et al* 1976, Mikke *et al* 1992) and for Mn–Cu (Wiltshire *et al* 1985). The main observations are as follows.

(1) For temperatures near T_N the SWs are overdamped.

(2) The data confirm that SW velocity depends linearly on the order parameter, as predicted by the RPA calculation by Sato and Maki (1976), in a lower temperature range but not close to T_N.

(3) We do not observe any special temperature dependence of the SW parameters connected with the proximity of the alloy concentration to the phase boundary region.

Acknowledgments

The authors are grateful to Professor E Z Vintaykin, Professor V A Udovenko and Dr S Y Makushev of Institute of Metal Physics, Moscow for preparing the sample and for the x-ray investigations of its crystalline structure. This work was supported by the State Committee for Scientific Research under the KBN contract no PB 2 0044 91 01.

References

Bozorth R M 1951 *Ferromagnetism* (Princeton, NJ: Van Nostrand) pp 243, 315–16
Cade M A and Young W 1977 *Adv. Phys.* **26** 393
——1980 *J. Phys. F: Met. Phys.* **10** 2035
Dushanek H, Mohn P and Schwarz K 1989 *Physica* **161B** 139
Gillan M J 1973 *J. Phys. F: Met. Phys.* **3** 1874
Hennion B, Hutchings M T, Lowde R P, Stringfellow M W and Tocchetti D 1986 *Proc 2nd Gatlinburg Conf. on Neutron Scattering* p 825
Holden T M, Mikke K, Fawcett E and Fernandez-Baca J 1992 *Proc. Int. Conf. Physics of Transition Metals* (Singapore: World Scientific) p 644
Honda N, Tanji Y and Nakagawa Y 1976 *J. Phys. Soc. Japan* **41** 1931
Ishikawa Y 1975 *Science Reports of the Tohoku University Series I* vol LVIII, pp 152–98
Jankowska-Kisielińska J, Mikke K and Milczarek J J 1995 *J. Magn. Magn. Mater.* **140–144** 1973
Jo T and Hirai K 1986 *J. Phys. Soc. Japan* **55** 2017
Kawarazaki S, Fujita K, Yasuda K, Sasaki Y, Mizusaki T and Hirai A 1988 *Phys. Rev. Lett.* **61** 471
Liu S H 1970 *Phys. Rev.* B **2** 2664
Long M W and Bayri A 1993 *J. Phys.: Condens. Matter* **5** 7719
Long M W and Yeung W 1986 *J. Phys. F: Met. Phys.* **16** 769
Lowde R D, Harley R T, Saunders G A, Sato M, Scherm R and Underhill C U 1981 *Proc. R. Soc.* A **374** 87
Mikke K, Holden T M, Fawcett E and Jankowska-Kisielinska J 1991 *Physica* **174B** 43
Mikke K, Jankowska-Kisielińska J and Jaworska E 1992 *Physica* **180B & 181B** 247
Mikke K, Milczarek J J, Udovenko V A, Jaworska E and Vintaikin E Z 1989 *Physica* **156B & 157B** 718
Mikke K, Milczarek J J, Vintaikin E Z and Udovenko V A 1987 *Acta Magn. Suppl.* **87** 254
Moze O and Hicks T J 1979 *J. Magn. Magn. Mater.* **14** 250
——1982 *J. Phys. F: Met. Phys.* **12** 1
Oguchi T and Freeman A J 1984 *J. Magn. Magn. Mater.* **46** L1
Oleś A, Kajzar F, Kucab M, Sikora W 1976 *Magnetic Structures Determined by Neutron Diffraction* (Kraków: Państwowe Wydawnictwo Naukowe) pp 490, 492–3
Sato M, Lowde R D, Saunders G A and Hargreave M M 1981 *Proc. R. Soc.* A **374** 115
Sato H and Maki K 1974 *Int. J. Magn.* **6** 183
——1976 *Prog. Theor. Phys.* **55** 319
Tajima K, Ishikawa Y, Endoh Y and Noda Y 1976 *J. Phys. Soc. Japan* **41** 1195
Vintaykin E Z, Udovenko V A, Litvin D F, Makushev S Yu and Dmitriev V B 1985 *Izvest. Vyssh. Ucheb. Zaved. Fizika* no 5 (Tomsk: Izdatelstvo Tomskogo. Universiteta) pp 104–18 (in Russian)
Wiltshire M C K, Elcombe M M and Howard C J 1985 *J. Phys. F: Met. Phys.* **15** 1595
Yeung W 1988 *Physica* **149B** 185